Pergamon

Acta mater. Vol. 46, No. 9, pp. 3033–3046, 1998

Printed in Great Britain
PII: S1359-6454(98)00016-0
1359-6454/98 $19.00 + 0.00

SHEAR LOCALIZATION AND CHEMICAL REACTION IN HIGH-STRAIN, HIGH-STRAIN-RATE DEFORMATION OF Ti–Si POWDER MIXTURES

H. C. CHEN, J. C. LASALVIA, V. F. NESTERENKO and M. A. MEYERS

Department of Applied Mechanics and Engineering Sciences, University of California, San Diego, La Jolla, CA 92093, U.S.A.

(Received 19 June 1997; accepted 19 December 1997)

Abstract—Ti–Si mixtures were subjected to high-strain-rate deformation at a pressure below the threshold for shock-wave initiation. Whereas the collapse of interparticle pores did not initiate reaction, regions of localized macro-deformation initiated reaction inside shear bands at sufficiently high strains ($\gamma \sim 10$), and propagation of the reaction through the entire specimen at higher strains ($\gamma \sim 20$–40). This study demonstrates that temperature increases in shear localization regions can initiate chemical reaction inside a reactive powder mixture. The shear band spacing was ~0.6–1 mm. Thermodynamic and kinetic calculations yield the reaction rate outside the shear bands, in the homogeneously deformed material, which has a maximum value of 20 s^{-1} at 1685 K. © *1998 Acta Metallurgica Inc.*

1. INTRODUCTION

There has been considerable interest, in the past thirty years, on mechanically induced chemical reactions [1–3]. The most striking development has been the shock induced synthesis of diamond from graphite, by DeCarli and Jamieson [4]. Two schools-of-thought developed, regarding the initiation of chemical reactions during shock compression: (a) the solid-state approach, according to which the high density of defects produced in shock compression, in combination with high pressures and temperatures, produced a solid-state reaction [2, 5, 6]; (b) the solid–liquid approach, according to which melting of one of the components of a reactive mixture was a prerequisite to initiate the reaction [7–13].

Shock-induced chemical reactions in silicide systems have been investigated in recent years. Vreeland and coworkers [7–10] proposed that chemical reactions were initiated under shock compression, when the shock energy was of sufficient amplitude to melt one of the mixture components. Meyers and coworkers [11–13] observed that small spherical $NbSi_2$ products form at the interface between Nb and Si, and are expelled into the molten silicon. Similar results can also be observed in the Mo + Si mixture [14, 15]. Vreeland and coworkers [16] applied shock energies slightly lower than the threshold energy on the Ti–Si mixture, and observed solid-Ti/molten-Si interfaces in small localized regions. Spherical reaction products ($TiSi_2$) were also formed at the Ti particle/Si liquid interface. Recent observations confirm the reaction mechanism not only for Nb + Si and Mo + Si systems, but also for other metal + Si systems.

The importance of shear deformation on chemical reactions was first demonstrated by Bridgman [17–20]; he showed that shear deformation, superimposed on hydrostatic loading, decreases the critical pressure for initiating chemical reactions. Vereshchagin and coworkers [21, 22] applied this technique and made the following observations: pressure combined with shear deformation can accelerate polymorphic transformations, lower the temperature for phase transitions, and decompose some compounds. Teller [23] hypothesized that shear deformation at high pressures can play a decisive role in accelerating chemical reactions, particularly, converting an exothermic reaction into an explosive process. Enikolopyan and coworkers [24–26] used a Bridgman anvil cell to study organic and inorganic chemical reactions under high pressures with shear deformation. Complete reactions in some materials only occurred with superimposed shear deformation, whereas in other materials reactions stopped after shear deformation was interrupted. These studies confirmed the earlier work by Bridgman [17–20].

Under shock compression, the combination of high pressure and temperature can cause powders to undergo plastic deformation, fluid-like flow, and mechanical mixing which can speed chemical reactions. The influence of post shock-shear deformation on chemical reaction under dynamic loading was accidentally observed by Yu [27] and Yu *et*

al. [28] in shock experiments carried out in the cylindrical geometry and in a gas gun. Potter and Ahrens [29] observed chemical reaction in oblique impact experiments between Al_2O_3 and MgO, with the formation of $MgAl_2O_4$. Recent results by Nesterenko *et al*. [30–33] show that chemical reactions in Ti + Si and Nb + Si powder mixtures can occur in a narrow band (width ~5–20 μm) produced by shear localization without essential influence of shock loading.

Krueger and Vreeland [8] proposed that a shock threshold energy is needed to initiate the reaction. This criterion was generalized to incorporate the effect of localized plastic deformation by Meyers *et al*. [15]; the total energy (shock energy plus energy inside shear localization area after passage of shock wave) was used in the computation, and initiation of reaction was consistent with the energy to melt Si.

The principal objectives of this paper are: (a) to investigate the behavior of Ti–Si mixture below the deformation threshold for chemical reaction in conditions of high-strain, high-strain-rate deformation and (b) to establish whether reaction, initiating at shear bands, could propagate into the mixture.

2. EXPERIMENTAL TECHNIQUES

A Ti–Si (74 wt%–26 wt%) powder mixture in its stoichiometric composition of compound Ti_5Si_3, was used in this research. This compound had been investigated in earlier shock experiments [27, 7–10] and it was therefore thought that it was a good initial composition for comparison purposes. Nevertheless, the Ti–Si phase diagram indicates a number of additional compounds. The enthalpy of reaction ΔH is [34]:

$$5\mathrm{Ti} + 3\mathrm{Si} \longrightarrow \mathrm{Ti_5Si_3} \quad \Delta H = -580\ \mathrm{kJ/mol}.$$

The powders (from CERAC) had sizes of −325 mesh ($<44\ \mu$m), high purity ($>99.5\%$) and irregular shape. Meyers *et al*. [12] and Yu [27] calculated the threshold pressure for reaction at 65% initial density and obtained a value of 1.5 GPa for Ti_5Si_3. This calculation is based on the Krueger–Vreeland criterion [8].

The thick-walled cylinder method, which was developed by Nesterenko *et al*. [35, 36] for the investigation of high-strain, high-strain-rate deformation of solid materials and modified for the study of inert and reactive porous powder mixtures [30, 31] was used in this investigation. The schematic of the set-up is presented in [30, 31]. Detonation is initiated at the top of the charge and propagates along the cylinder axis. The powder is first consolidated by a low amplitude explosive charge. An orifice is then drilled along the cylinder axis and a second explosive event is carried out. This second explosive produces significant plastic deformation in the densified powder layer. The velocity of the inner cylinder surface and the collapse time were measured by a non-contact electromagnetic method [36].

Figure 1 shows the details or the set-up. A porous powder (initial density of Ti–Si mixture was ~35% of theoretical density) was initially placed in a tubular cavity between a central copper rod (diameter of 16 mm) and an outer copper tube (inner diameter of 20 mm and outer diameter of 31 mm). Explosive 1 (mixture of ammonite and sand in 3:1 volume ratio, Fig. 1(a)) with low detonation velocity (2.8–3 km/s) was used to densify the powder. After densification, the density of mixture became ~80% of theoretical value. No significant shear localization or chemical reaction was observed after this stage because the global deformation is sufficiently small (final diameter of inner surface of driving copper cylinder is equal to 18–19 mm). This stage produced mainly the densification of the powder. A cylindrical hole with diameter 11 mm was drilled along the longitudinal axis of the copper rod and this composite cylinder was collapsed by the detonation of a second cylindrical explosive charge (ammonite, Fig. 1(b)) with a detonation velocity of 4–4.2 km/s, an initial density of 1 g/cm^3, and an outer diameter of 60 mm. This second explosive loading produced significant plastic deformation in densified porous layer which was highly localized in shear bands and not homogeneously distributed (Fig. 1(c)). To precisely tune the global strains, a cylindrical copper rod was inserted in the central orifice after Explosive 1 (Fig. 1(d)). This was intended to provide the critical initiation and propagation condition for shear localization and chemical reaction.

The global material strain can be obtained quantitatively from the strains in the incompressible copper shell driving the collapse process. The strain state in the uniformly deformed incompressible material is pure shear [31, 37]. The radial and tangential true strains (ε_{rr} and $\varepsilon_{\varphi\varphi}$) for the copper shell, before the onset of localization, can be estimated by knowing the initial and final radii, r_i and r_f, at a general point:

$$\varepsilon_{rr} = -\varepsilon_{\varphi\varphi} = \ln\left(\frac{r_i}{r_f}\right). \tag{1}$$

The true strains in the inner and outer surfaces of the initial porous tubular layer can be found from equation (1). The final radii R (or R_1) and initial radius R_0 (or R_{10}) (Fig. 1) are experimentally measured and the value of r_i, which corresponds to a preselected value of r_f, can be calculated by using the conservation of mass:

$$r_i^2 = r_f^2 + R_0^2 - R^2 = r_f^2 + R_{10}^2 - R_1^2 \tag{2}$$

where R and R_1 are the final radii of the inner hole and outer cylinder surface. The effective strains can

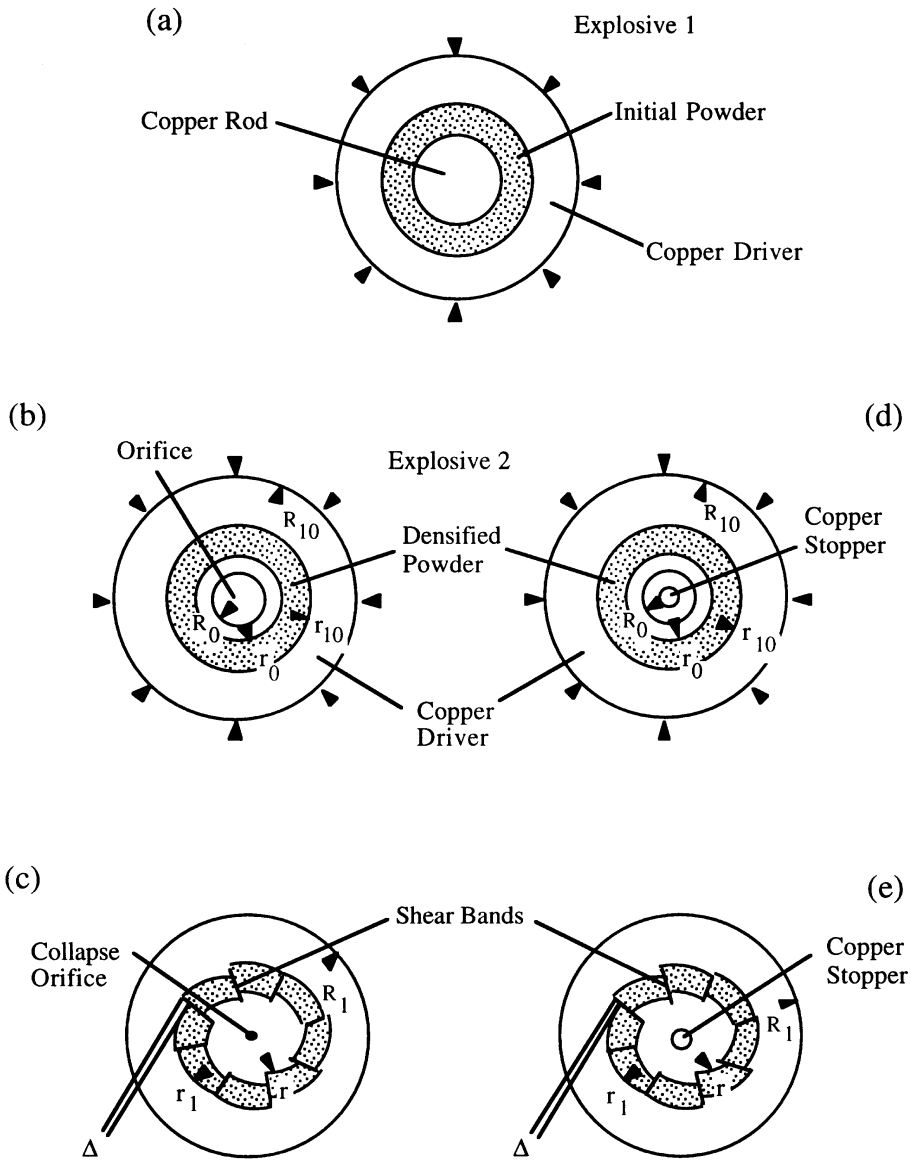

Fig. 1. Geometry and sequence of deformation events in thick-walled cylinder method: (a) initial geometry, densified by explosive 1; (b) densified powder with central orifice cylinder collapsed by explosive 2; (c) final geometry; (d) densified powder with copper stopper; (e) final geometry. Copper stopper in (d) and (e) as well as diameter of the orifice R_0 allows precisely tuned global deformation.

be calculated ($\varepsilon_{zz}=0$) according to:

$$\varepsilon_{\text{eff}} = \frac{\sqrt{2}}{3}[(\varepsilon_{rr}-\varepsilon_{\varphi\varphi})^2+(\varepsilon_{\varphi\varphi}-\varepsilon_{zz})^2+(\varepsilon_{zz}-\varepsilon_{rr})^2]^{1/2} = \frac{2}{\sqrt{3}}\varepsilon_{rr}. \quad (3)$$

The global strains in copper at the boundary with the porous layer outside the shear localization region can be estimated by using equation (1) and equation (3). Table 1 shows the calculated results.

The stress state in these plane-strain experiments is very difficult to control, because the stresses are determined by the material strength during plastic flow, and they depend on temperature, strain and strain rate. Two principal features of this method should be mentioned:

(i) The weak shock waves propagating in the material during the first stage of collapse have no noticeable influence on the chemical reaction; their amplitudes are less than 1 GPa. This step of loading resulted in the densification of mixture from 35% up to ~80% of theoretical density.

(ii) The shock pressures for both stages were kept below the threshold shock pressure for reaction initiation. Vreeland *et al.* [16] demonstrated that the shock energy threshold E_{sh} for complete reaction in the porous mixture 5Ti + 3Si depends upon powder particle size and initial porosity: $E_{\text{sh}}=375$ J/g

Table 1. Global strains for Ti–Si mixture

Materials		Ti–Si			
Copper stopper size (mm)		0	1.5	3	6
After explosive 1	ε_{rr} ($-\varepsilon_{\varphi\varphi}$)	0.08 ± 0.01	0.07 ± 0.01	0.07 ± 0.01	0.07 ± 0.01
	ε_{eff}	0.09 ± 0.01	0.08 ± 0.01	0.09 ± 0.01	0.09 ± 0.01
After explosive 2	ε_{rr} ($-\varepsilon_{\varphi\varphi}$)	0.32 ± 0.01	0.31 ± 0.01	0.29 ± 0.01	0.21 ± 0.01
	ε_{eff}	0.38 ± 0.01	0.35 ± 0.01	0.33 ± 0.01	0.24 ± 0.01

(shock pressure 2.65 GPa) for larger particles (−150 mesh) is 80% larger than for smaller particles at the same porosity (0.49) and a decrease in initial porosity from 0.49 to 0.4 resulted in 75% increase of E_{sh} for both powders. A constant threshold energy of $E_{sh} = 100$ J/g was assumed for mixture 5Ti + 3Si resulting in a range of critical shock pressures to initiate reaction from 1 GPa at porosity 0.5 to 3 GPa at porosity 0.2 [33]. A separate experiment was conducted for Stage 2 with the same type of explosive loading but without global plastic deformation. There was no evidence of reaction. Thus it can be concluded that pressure effects can be neglected to a first approximation and chemical processes are mainly strain controlled.

3. RESULTS AND DISCUSSION

Four different deformation conditions were applied to Ti–Si mixtures. The global strains in the inner layer were 0.24, 0.33, 0.35, 0.38 by using copper stopper diameters, D, equal to 6, 3, 1.5, and 0 mm, respectively. The details are shown in Table 1. The global strain rates are calculated by [31] and the average values are very close and about 2×10^4 s^{-1}. Shear localization is seen from the steps at the internal and external surfaces of the cylindrical specimens. Profuse shear localization (Fig. 2) can be seen in samples with $\varepsilon_{eff} \approx 0.33$, 0.35, 0.38, while the sample with $\varepsilon_{eff} \approx 0.24$ showed only the onset of shear bands (Fig. 2(a) marked with arrows). From this result, one can conclude that

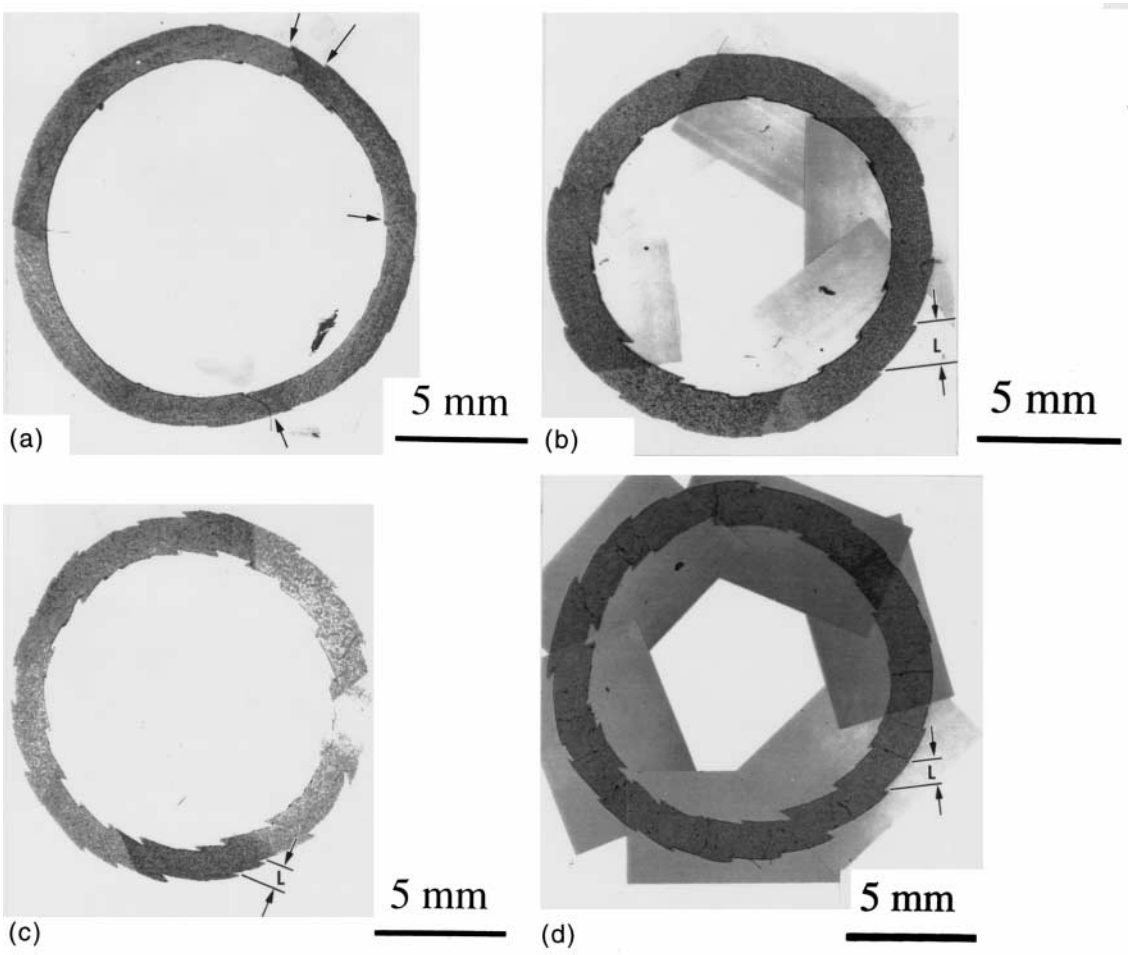

Fig. 2. Ti–Si mixtures under different deformation conditions: (a) $\varepsilon_{eff} \approx 0.24$; (b) $\varepsilon_{eff} \approx 0.33$; (c) $\varepsilon_{eff} \approx 0.35$; (d) $\varepsilon_{eff} \approx 0.38$.

Table 2. Global and local shear properties for Ti–Si mixture

Effective global strain, ε_{eff}	0.24	0.33	0.35	0.38
Displacement, Δ (μm)	0	100–200	150–400	200–600
Shear band thickness, δ (μm)	~0	10–15	10–15	—
Local shear strain, γ	0	10–20	15–40	20–60
Local shear strain rate, $\dot{\gamma}$ (s^{-1})	0	$\sim 10^6$	$\sim 10^6$	$\sim 10^6$
Total tangential strain, e_t	−0.166	−0.214	−0.239	−0.239
Homogeneous strain, e_h	−0.166	−0.156	−0.151	−0.112
Inhomogeneous strain, e_s	0	−0.058	−0.088	−0.127

shear localization developed at a global effective strain between 0.2 and 0.3. The angle between the shear localization regions and the radial direction is close to 45°, the same as in alumina samples [38]. This demonstrates that plastic flow in these materials is rather pressure insensitive. Two orientations, either clockwise or counterclockwise spirals, are observed.

Using the ratio of the displacement, Δ, and the thickness of the shear bands, δ, one can evaluate the shear strain inside shear localization regions, which are deforming in simple shear. The shear displacements, Δ, shear band thicknesses, δ, local shear strains, γ, and local shear strain rates, $\dot{\gamma}$, are listed in Table 2. The local shear strain rate is calculated by:

$$\dot{\gamma} = \frac{\gamma}{\tau}$$

where τ is the time of the deformation process and is equal to ~8 μs [35, 36]. The total global tangential strain, e_t, homogeneous strain, e_h, and inhomogeneous strain due to shear localization, e_s, are calculated by [38]. The calculated values are listed in Table 2.

The microstructural observations for the Ti–Si system are shown in Figs 3–6. There is no significant difference after the densification stage (explosive event 1) among all sets of specimens and the densities are 65–90% of the theoretical value. After explosive event 2 with varying diameters of the central copper stopper (varying global strain conditions), the structures are quite different. Only the beginning of shear localization was found for global strain, $\varepsilon_{eff} \sim 0.24$ (Fig. 3). Although there are no well developed shear bands at $\varepsilon_{eff} \sim 0.24$, small localized regions of shear concentration were observed (Fig. 3(b)). This phenomenon is probably due to material non-uniformity initiated, for example, by the fracture of Si particles. When the global strain increases to ~0.33 and 0.35, shear localization becomes evident (Fig. 4(a) and Fig. 5(a)). At $\varepsilon_{eff} \sim 0.33$, fracturing and extensive plastic flow of Ti particles are observed inside shear localization regions (Fig. 4(b)). This implies that material flow is unstable during deformation. Spherical partially reacted products were observed only inside shear localization regions (shown by arrows in Fig. 4(b)). These reacted products were Ti-rich compounds as determined by EDS analysis. These reaction products are similar to the spherules observed after shock compression of powders by Vecchio *et al.* [13] and Vreeland *et al.* [16].

At $\varepsilon_{eff} \sim 0.35$, the reactions inside shear localization regions are completed, as shown in Fig. 5(b). At the reaction interface, which is quenched by the surrounding medium, small spherules (~0.2–0.5 μm diameter) can be seen (Fig. 5(c)) and are marked by arrows. These spherules are evidence that the reaction propagation mechanism is similar to the one observed by Yu and Meyers [11] under shock compression and to the one discussed by LaSalvia *et al.* [39] under conventional SHS. The voids and cracks in the reaction products are due to solidification shrinkage. This can be explained by the liquid state of the products after reaction. At ε_{eff}~0.38, in some experiments, the reaction propagated throughout the whole specimen, except in the triangular areas produced by discontinuity in displacement due to shear localization (Fig. 6(a)). Only cracks were left as the main feature of shear localization (Fig. 6(b)), as a result of solidification and shrinkage of molten reacted products. The unreacted triangular areas are due to rapid heat extraction by the copper walls at an angle of 45°. These fully reacted products were identified by X-ray diffraction analysis and the results coincide with the major peaks for Ti_5Si_3. The d spacings for the two strongest peaks were 2.204 A (for (211)) and 2.124 A (for (112)), with corresponding lattice parameters of $a = 7.35$ A and $c = 5.49$ A. In comparison the JCPDS reports data of 2.202 A (for (211)) and 2.116 A (for (112)), with corresponding lattice parameters of $a = 7.44$ A and $c = 5.143$ A(hexagonal structure; $P6_3/mcm$). It is therefore concluded that the reaction product is indeed Ti_5Si_3. In accordance with this, the microhardness for densified Ti–Si mixtures is 180 VHN, whereas for shear deformed and reacted Ti–Si mixtures, it is 910 VHN. This result additionally confirms that the structures after shear deformation are quite different from the densified one, and that a new compound was formed.

The second explosive loading event was also conducted without creating a central orifice. After this shock loading without collapse process, no shear localization and chemical reaction were observed. This confirms that the chemical reaction are truly strain controlled in our experiments.

The voids and microcracks, shown in Fig. 6(b), indicate that the reacted product Ti_5Si_3 has melted

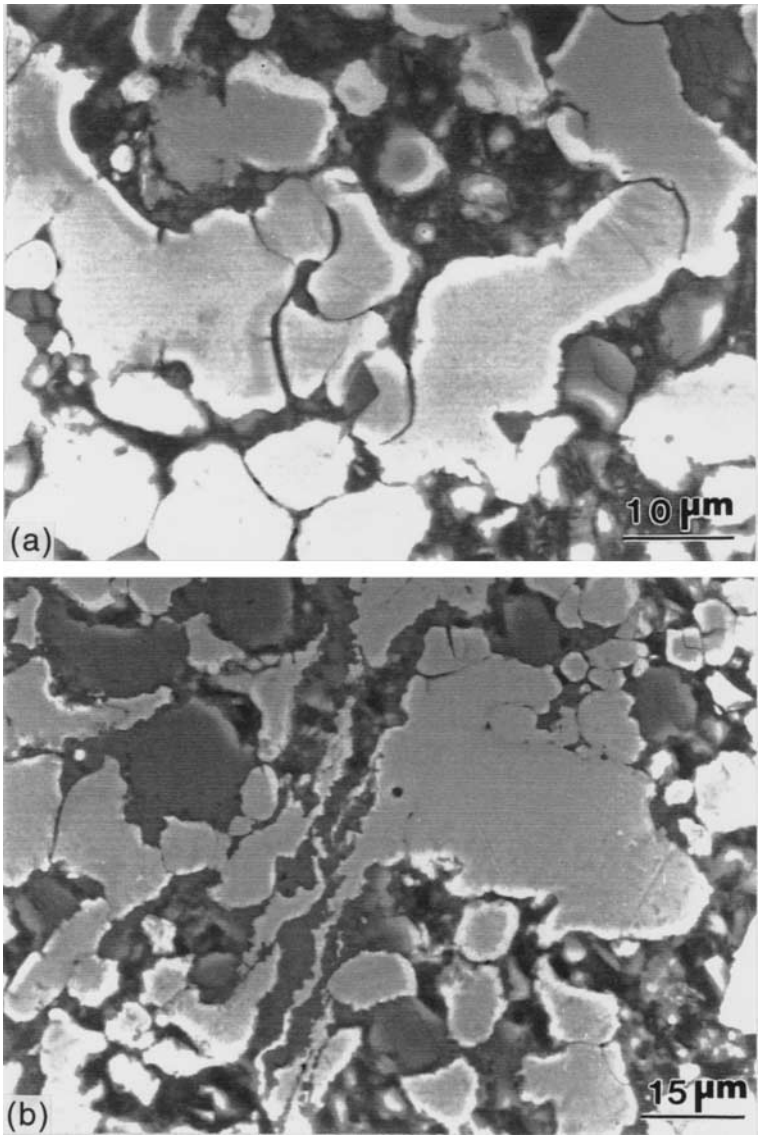

Fig. 3. Microstructure in Ti–Si mixture at $\varepsilon_{\text{eff}} \approx 0.24$ (a) typical area; (b) shear flow regions.

and resolidified. The reaction is initiated inside the shear localization regions as a result of extensive plastic flow. The heat in the environment of shear regions after reaction initiation must have been enough to ensure the melting of Ti_5Si_3, which occurs at 2403 K. This high local temperature is due to two effects: heat produced by plastic work conversion and heat released from chemical reaction. The increase in temperature from plastic work ΔT_s can be estimated by:

$$\Delta T_s = \frac{1}{\rho C_{p1}} \int_0^{\gamma} \tau \, d\gamma \tag{4}$$

where ρ is the theoretical density of solid mixture which is equal to 3.85 g/cm^3, C_{p1} is the heat capacity of unreacted densified powder, and $\tau \, d\gamma$ is the deformation work. The heat capacity can be estimated by mass fraction m_{Ti} of Ti and m_{Si} of Si powder:

$$C_{p1} = m_{Ti} C_{p1}(\text{Ti}) + m_{Si} C_{p1}(\text{Si}) \tag{5}$$

The heat capacities are 0.523 J/g·K and 0.70 J/g·K for titanium and silicon, respectively. The mass fractions are: $m_{Ti} = 0.74$ and $m_{Si} = 0.26$. Therefore, the average heat capacity for unreacted densified powder is 0.57 J/g·K. To obtain the deformation work, the flow stress of material (σ) should be estimated. To a first approximation, the Johnson–Cook equation [40] can be used. Ignoring work hardening, the flow stress is:

$$\sigma = \sigma_0 \left(1 + C \log \frac{\dot{\varepsilon}}{\dot{\varepsilon}_0}\right) \left[1 - \left(\frac{T - T_r}{T_m - T_r}\right)^m\right] \tag{6}$$

where σ_0 is the flow stress at a reference strain rate $\dot{\varepsilon}_0$ and temperature T_r, C is the strain rate sensitivity, m is the thermal softening parameter, T_m is

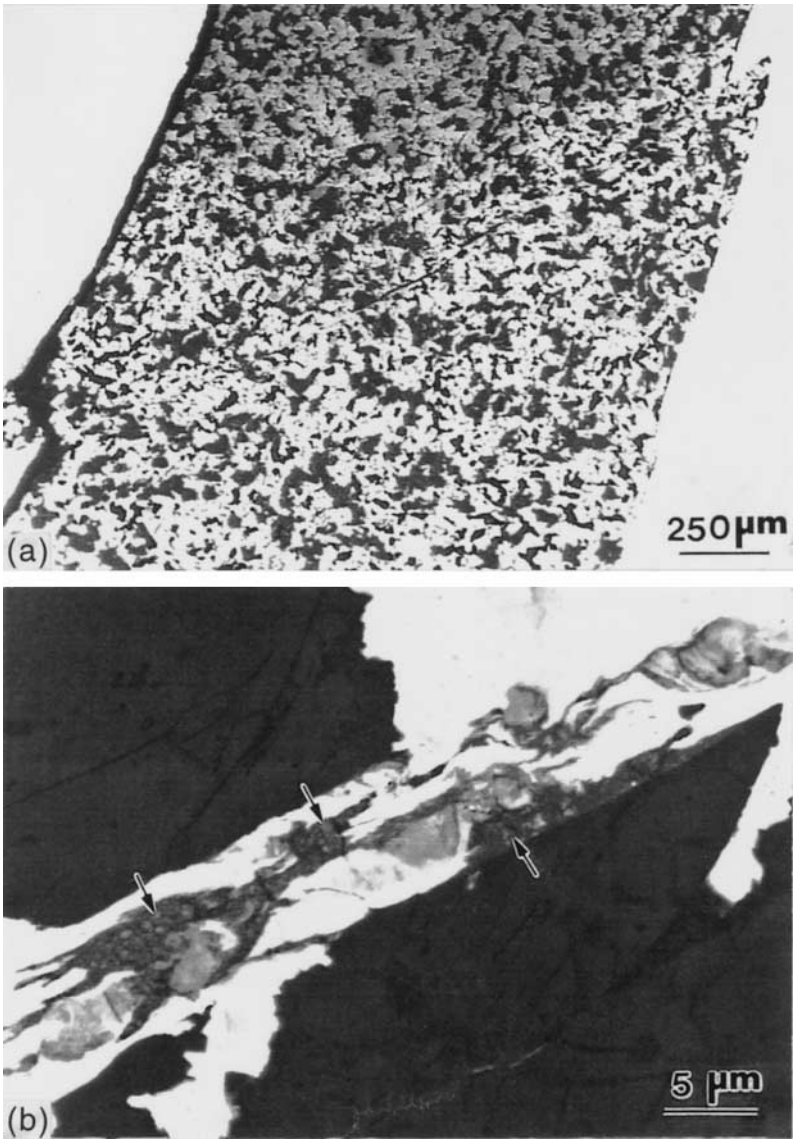

Fig. 4. Shear band structure in Ti–Si mixture at $\varepsilon_{\text{eff}} \approx 0.33$ (a) overall view of shear band; (b) microstructure of shear bands (arrows show the partially reacted particles).

the melting temperature and T is current temperature. A linear softening ($m = 1$) and conventional strain-rate sensitivity ($C = 1$) [15] are assumed, and the melting temperature is taken as the weighted average between Ti and Si ($T_{\text{m}} \approx 1876$ K). If the reference strain rate and temperature are taken as $1\ \text{s}^{-1}$ and 300 K, and the flow stress for mixture is assumed to be the weight average between Ti (170 MPa) and Si (90 MPa), resulting in $\sigma_0 \approx 150$ MPa. Equation (6) can be rewritten as:

$$\sigma = 1050 \times \left(1 - \frac{T - 300}{1600}\right). \tag{7}$$

Taking $\tau = \sigma/2$ and substituting into equation (4), where $\Delta T_{\text{s}} = T - 300$ K, one can obtain that:

$$T = 300 + \frac{240\gamma}{1 + 0.15\gamma}. \tag{8}$$

Fig. 7 shows the temperature as a function of local shear strain.

Experimental results show that the reactions occurred for the specimens at $\varepsilon_{\text{eff}} \approx 0.33$, 0.35, 0.38. The shear strains generated in the shear bands are of the order of 10–60. It is possible to estimate the shear strain at which the temperature is equal to the melting point of Si, 1685 K; it corresponds, in Fig. 7, to shear strain of ~40. The heat of reaction at different temperatures can be calculated by [43]:

$$\Delta H_T = \Delta H_{298} + \int_{298}^{T} \Delta C_{\text{p}}\, \text{d}T \tag{9}$$

$$\Delta C_{\text{p}} = C_{\text{p}}(\text{Ti}_5\text{Si}_3) - 5C_{\text{p}}(\text{Ti}) - 3C_{\text{p}}(\text{Si}) \tag{10}$$

$$C_p(Ti_5Si_3) = \begin{cases} 196.439 + 44.769 \times 10^{-3}T - 2.008 \times 10^6 T^{-2} & \text{at } T < 2403 \text{ K} \\ 270 & \text{at } T > 2403\ K \end{cases} \quad (11)$$

$$C_p(Ti) = \begin{cases} 22.238 + 10.205 \times 10^{-3}T - 0.008 \times 10^6 T^{-2} & \text{at } T < 1166 \text{ K} \\ 17.405 + 10.314 \times 10^{-3}T - 0.096 \times 10^6 T^{-2} & \text{at } 1166 \text{ K} < 1939 \text{ K} \\ 47.237 & \text{at } T > 1939 \text{ K} \end{cases} \quad (12)$$

$$C_p(Si) = \begin{cases} 22.811 + 3.870 \times 10^{-3}T - 0.356 \times 10^6 T^{-2} & \text{at } T < 1685 \text{ K} \\ 27.196 & \text{at } T > 1685 \text{ K} \end{cases}. \quad (13)$$

If T is higher than the melting points of reactants or products, the latent heat of fusion, L_m, should be considered and added to the right hand side of equation (9). The melting points and latent heat of fusion for Ti, Si and Ti_5Si_3 are: $T_m = 1935$ K, $L_m = 18.6$ kJ/mol for Ti; $T_m = 1685$ K, $L_m = 50.2$ kJ/mol for Si; and $T_m = 2403$ K, $L_m = 178.88$ kJ/mol for Ti_5Si_3. From equations (9)–(13), the heats of reaction are: $\Delta H_{1350\ K} = -575$ kJ/mol, $\Delta H_{1685\ K} = -520$ kJ/mol, and $\Delta H_{1750\ K} = -520$ kJ/mol, corresponding to γ = 10, 40, and 60 respectively.

Assuming that the reaction is adiabatic, the adiabatic temperature, T_{ad} can be calculated by:

$$-\Delta H_T = \begin{cases} \int_T^{T_{ad}} C_{p2}\, dT & T_{ad} < T_m \\ \int_T^{T_m} C_{p2}\, dT + \nu L_m & T_{ad} \approx T_m \\ \int_T^{T_m} C_{p2}\, dT + L_m + \int_{T_m}^{T_{ad}} C_{p3}\, dT & T_{ad} > T_m \end{cases} \quad (14)$$

where ΔH_T is the heat of reaction at T, T_m ($\approx$2400 K) is the melting point of product Ti_5Si_3, ν is the fraction of Ti_5Si_3 product in the liquid phase, L_m (179 kJ/mol) is the latent heat of fusion for Ti_5Si_3, $C_{p2} \approx 196.44 + 0.045T - 2 \times 10^6/T^2$ J/mol K and $C_{p3} \approx 270$ J/mol K are the heat capacities of solid and liquid phase Ti_5Si_3, respectively [41–43]. The temperature inside shear bands is dependent on the value of local shear strain; the adiabatic temperatures for reaction at shear strains between 10 (T = 1350 K) and 60 (T = 1750 K) are 2500 to 3000 K. These results show that the reaction product, Ti_5Si_3, melts, since its melting point is equal to 2403 K.

The observations agree with the calculations; spherical reaction particles can be formed along heavily deformed Ti particles inside shear bands at γ = 10, as shown in Fig. 8. The presence of these spherules was also observed by Meyers and coworkers [11–15] in shock compression processing. These spherules are produced at the Ti (solid)–Si (liquid) interface, and are initially liquid. Interfacial energy spheroidizes the products, which subsequently solidify. The results suggest that Si is molten in this reaction region, and the initiation temperature for reaction is between 1685 K (melting point of Si) and 1945 K (melting point of Ti). The friction between Ti and Si particles also supplies heat to the interface and increases the temperature locally. Therefore, a mechanism of shear-assisted chemical reaction for Ti–Si system based on solid–liquid reaction is proposed:

(1) Ti particles are extensively deformed with shear localization. They are heated as a result of intense shear deformation and the material flow is unstable. These Ti foils have "fresh" surfaces without contamination by oxides.

(2) Si particles are molten and reaction initiates during flow or as a result of heat generated from mechanical work. This is similar to the "roller" model proposed for shock-induced reactions by Dremin and Breusov [43], shown in Fig. 9. The reaction proceeds along the Ti sliver–molten Si interface; thus, the Ti slivers are at least partially transformed into the reaction product.

(3) The reaction products are expelled away from the reaction interfaces in order to minimize interfacial energy, forming spherules. This is similar to the shock-assisted reaction mechanism [12] proposed by Meyers *et al.* [12–15].

(4) Reaction continues in places where temperatures are sufficiently high and then is quenched by thermal diffusion into the relatively cold surrounding material.

(5) When heat generation rate sufficiently high, reaction propagates throughout specimen.

In order to estimate the reaction rate in "uniformly" deformed material outside shear bands, one can use the unreacted triangle shown in Fig. 6(a) (see arrows) and Fig. 10(a). In this unreacted triangular region, the reaction rate was lower than the rate of heat loss and the reaction was therefore arrested. Thus, $\partial T/\partial t$ should be less than 0. From the conservation of energy, one can obtain:

$$\frac{\partial T}{\partial t} = \alpha \frac{\partial^2 T}{\partial x^2} + \frac{Q}{C_p}\frac{\partial \eta}{\partial t} < 0, \qquad \frac{Q}{C_p}\frac{\partial \eta}{\partial t} < -\alpha \frac{\partial^2 T}{\partial x^2}. \quad (15)$$

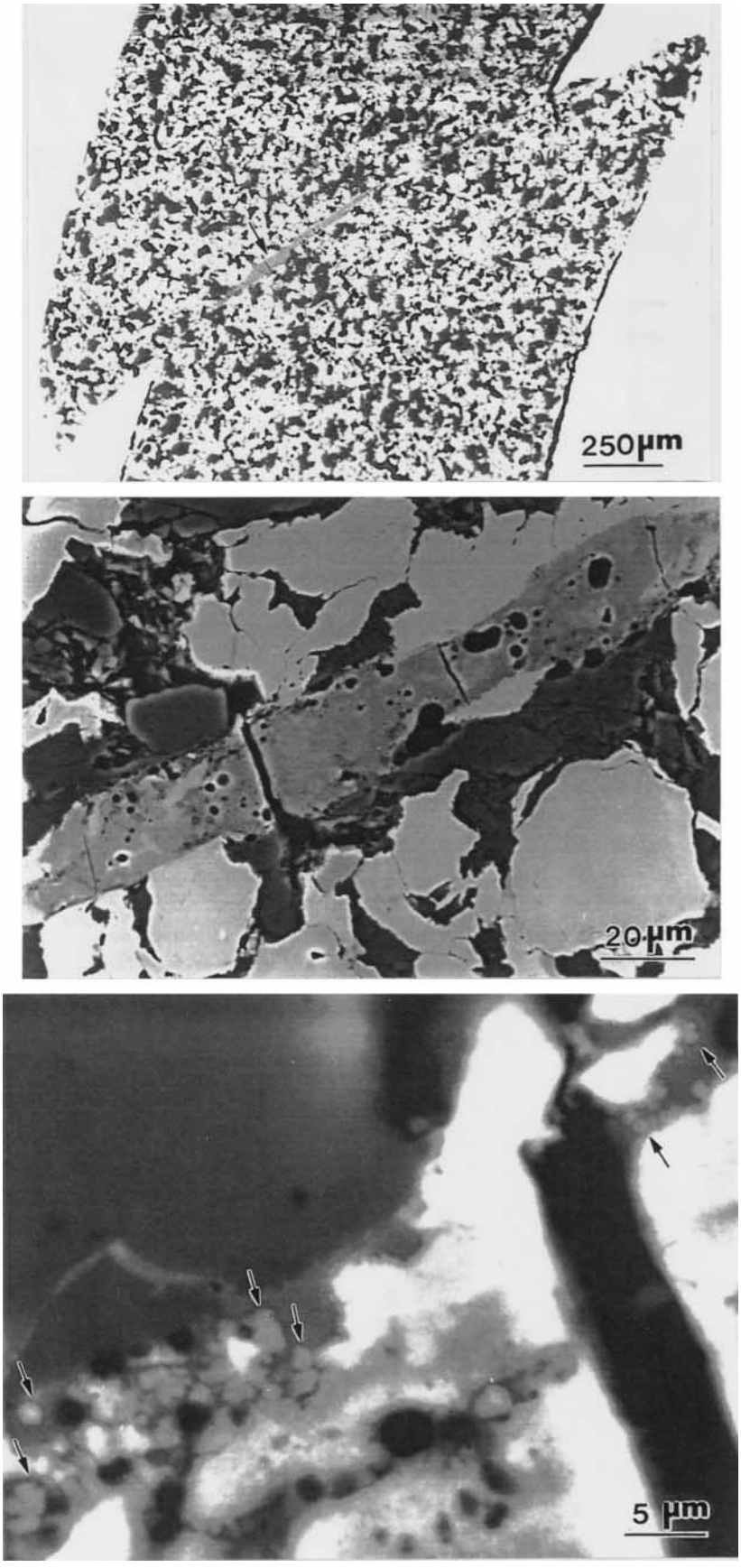

Fig. 5. Shear band structure in Ti–Si mixture at $\varepsilon_{eff} \approx 0.35$ (a) overall view of shear band; (b) complete reaction products inside shear bands; (c) close-up showing spherules at the interface of shear band with unreacted material.

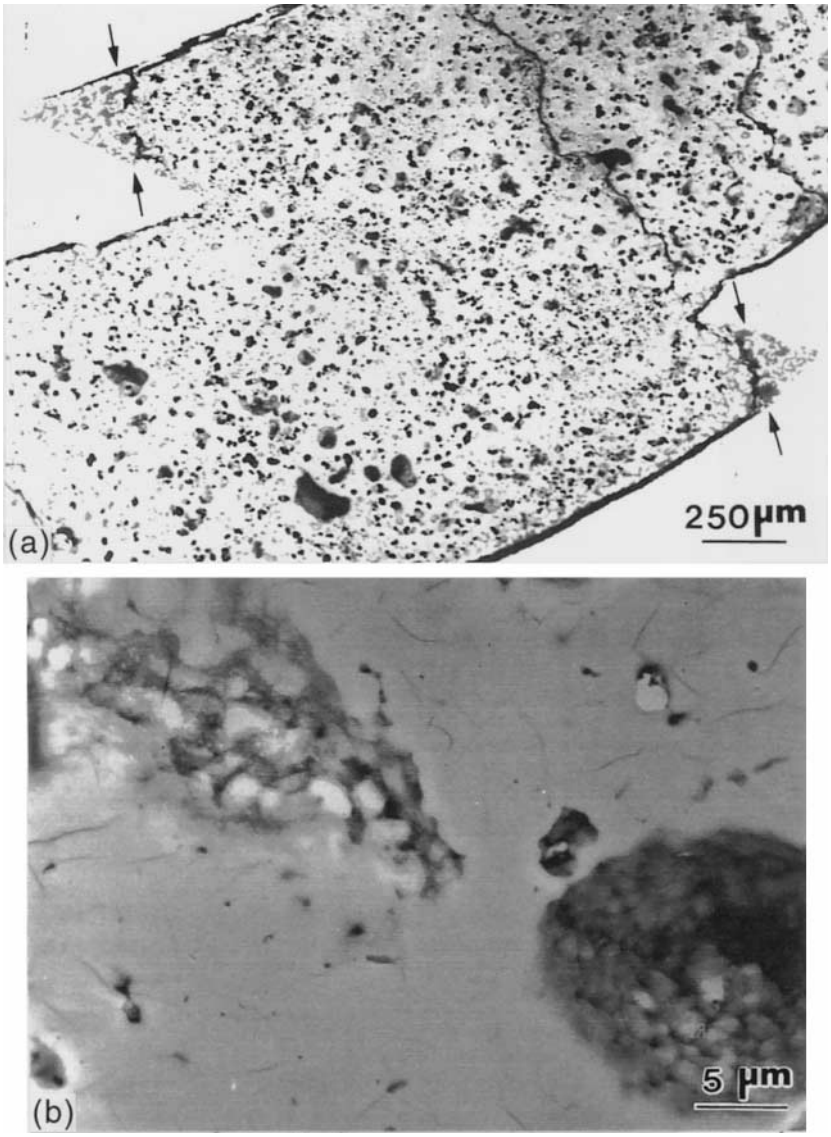

Fig. 6. Shear band structure in Ti–Si mixture at $\varepsilon_{\text{eff}} \approx 0.38$ (a) overall view of shear bands (arrows show the unreacted triangular regions); (b) fully reacted products with shear cracks.

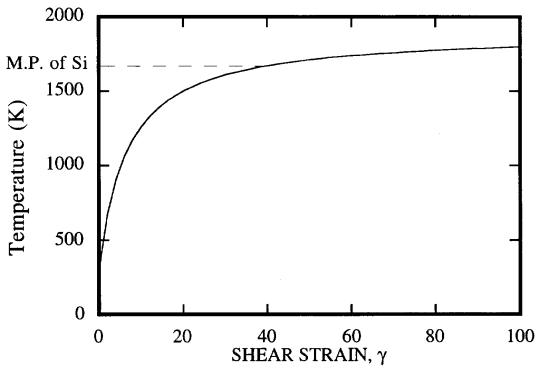

Fig. 7. Calculated temperature as a function of local shear strain.

The condition for reaction arrest can be written as follows:

$$\dot{Q}_{\text{r}} = Q\frac{\partial \eta}{\partial t} < -\alpha C_{\text{p}}\frac{\partial^2 T}{\partial x^2} \tag{16}$$

where ρ is the density (kg/m^3), C_{p} is the heat capacity (J/kg K), k is the thermal conductivity (W/m K), α is thermal diffusivity, η is the degree of conversion, $\partial\eta/\partial t$ is the reaction rate, Q is the reaction heat, and Q_{r} is the heat release rate of the reaction. Equation (16) allows evaluation of the heat release rate of the reaction from heat conductivity equation.

When the temperature reaches the adiabatic temperature T_{ad}, the heat release rate of the reaction $\dot{Q}_r$

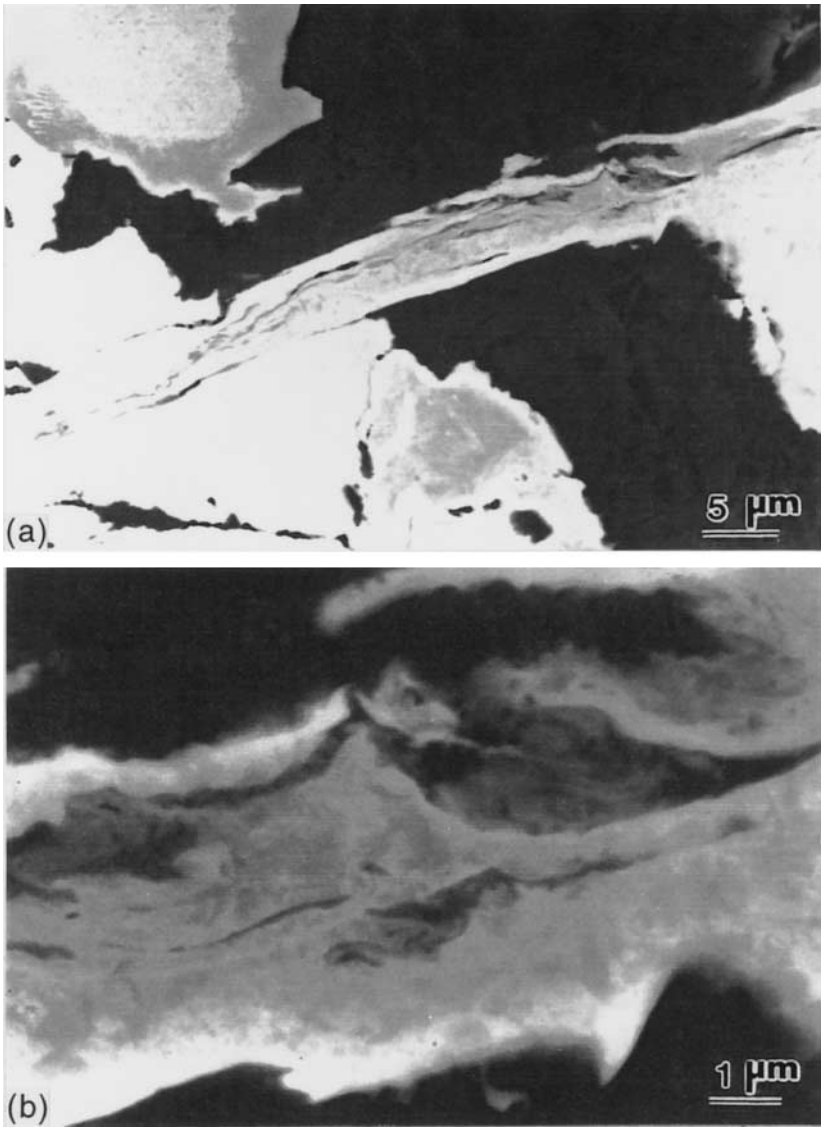

Fig. 8. Microstructure of shear band at $\gamma \sim 10$: (a) extensive deformation of Ti particles and spherical reacted particles; (b) interface between fractured Ti and reacted products.

is maximum [45]. The adiabatic temperature for $5Ti + 3Si \rightarrow Ti_5Si_3$ at room temperature is 2403 K [46]. Therefore, to estimate the reaction rate, it is assumed that the unreacted triangle

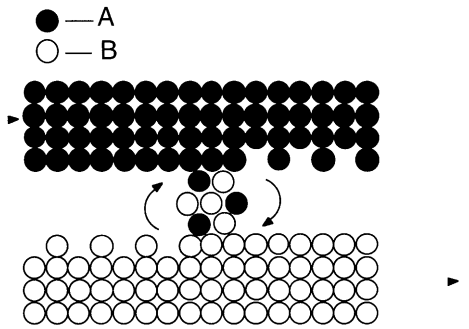

Fig. 9. Roller model for shear-induced chemical reactions. [44].

consists of a 5Ti + 3Si powder mixture at 2403 K; the temperature in copper is 300 K; and the fully reacted regions with Ti_5Si_3 compound are at 2403 K. Figure 10(b) shows the schematic illustration. In this case, only heat transfer is considered to calculate the cooling rate for this triangular region. A two-dimensional finite element program was used to calculate the temperature history according to the geometry represented in Fig. 10. The thermophysical properties are taken from [46] and Fig. 11 shows the calculated results at critical point 1 in this region, where reaction was apparently quenched by fast heat removal [39]. From the calculated temperature–time curve (Fig. 11(a)), one can estimate the cooling rate, which corresponds to the slope of the curve. The cooling rate varies as a function of time and is maximum at the inflection point of the curve in Fig. 11(a). The rate of heat

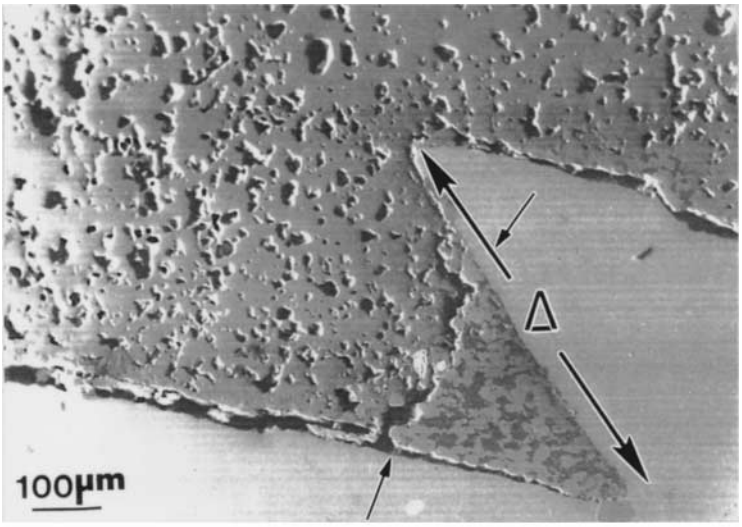

(a)

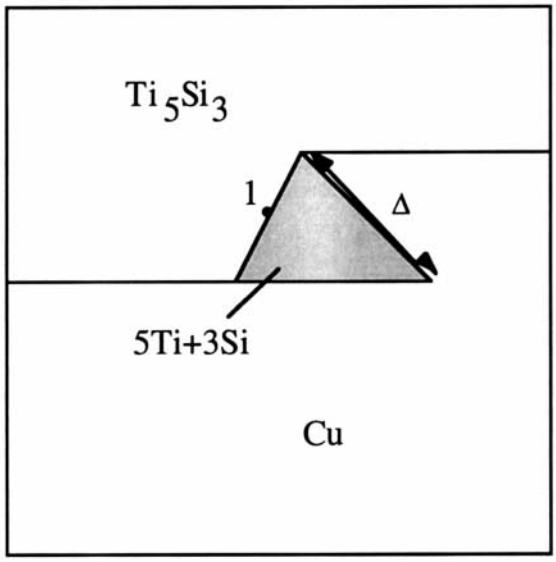

(b)

Fig. 10. (a) Unreacted triangular region at $\varepsilon_{\text{eff}} \approx 0.38$; (b) Schematic representation of a triangular region.

loss $\dot{Q}_{\text{loss}}$ is:

$$\dot{Q}_{\text{loss}} = C_{\text{p}} \frac{\partial T}{\partial t} = \alpha C_{\text{p}} \frac{\partial^2 T}{\partial x^2}. \tag{17}$$

The condition for reaction extinction is:

$$\dot{Q}_{\text{r}} < -\dot{Q}_{\text{loss}} \tag{18}$$

Fig. 11(b) shows the time-dependent rate of heat loss. The maximum $\dot{Q}_{\text{loss}}$ is equal to 4.5×10^5 J/g s. Therefore, the heat release rate for the reaction $5\text{Ti} + 3\text{Si} \rightarrow \text{Ti}_5\text{Si}_3$ should be less than this value.From equation (16), the maximum of reaction rate, $\partial\eta/\partial t$, can be calculated and is equal to 250 s^{-1} at $T = T_{\text{ad}} = 2403$ K. If an Arrhenius relationship is used for reaction kinetics

$$\frac{\partial \eta}{\partial t} = K_0 (1-\eta)^n \text{e}^{-E/RT} \tag{19}$$

then the coefficient K_0 can be estimated from the experimental data.

The activation energy E for the synthesis of Ti_5Si_3 is 125 kJ/mol [47] and the most reliable value of η is selected as 50% conversion [48, 49]. Assuming the reaction is first order ($n = 1$), then the rate constant, K_0, is calculated from equation (19) and equal to

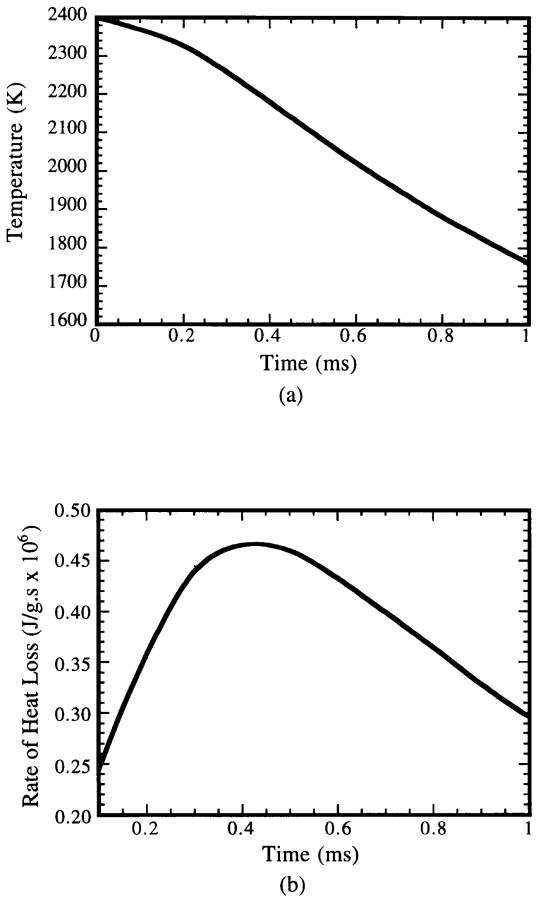

Fig. 11. Predicted temperature profile and rate of heat loss inside unreacted triangular region (point 1 in Fig. 10): (a) Temperature–time curve; (b) rate of heat loss–time curve.

$2.6 \times 10^5\ s^{-1}$. Since the reaction rate is a function of temperature (through the Arrhenius relationship), one can obtain curves shown in Fig. 12. It is instructive to calculate the reaction rates inside the shear bands from the Arrhenius equation with the parameters established above. Taking shear strains of 10 and 60, temperatures of 1350 K and 1750 K are obtained from Fig. 7, the corresponding reaction rates are $2\ s^{-1}$ and $30\ s^{-1}$, respectively. The characteristic time for shear-band formation and quenching is on the order of 10^{-5} s [30, 31]. If it is assumed that reaction occurs during deformation, then the rate of reaction inside the shear band must be on the order of $10^5\ s^{-1}$. It is many orders of magnitude higher than the rates calculated from the bulk. There are two possible reasons for this discrepancy:

(a) The reaction inside the band is truly shear assisted, i.e., it initiates at the end of plastic deformation and continues after deformation has ceased.

(b) The reaction rate within the shear band is orders of magnitude higher than in the bulk. The fact that particles are highly deformed and fractured, with creation of fresh interfaces is clearly suggestive of much higher reaction rates inside the bands.

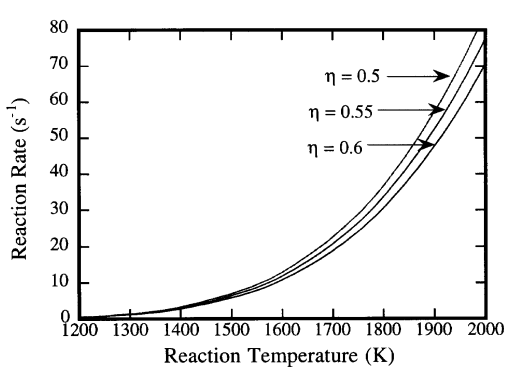

Fig. 12. Reaction rate vs temperature for 5Ti + 3Si system due to shear deformation.

4. CONCLUSIONS

(1) High-strain-rate plastic deformation of densified Ti–Si powder mixtures, inside the mechanical threshold for reaction initiation ($\varepsilon_{eff} \approx 0.24$–$0.38$, and $\dot{\varepsilon}_{eff} \approx 10^4\ s^{-1}$), was produced by low detonation velocity explosives. The pressure (< 1 GPa) is lower than the threshold value for shock-induced reaction. Shear localization is observed for global strains above 0.2.

(2) Chemical reactions initiate inside shear bands at $\varepsilon_{eff} \approx 0.33$. The reactions become more complete inside shear bands at $\varepsilon_{eff} \approx 0.35$, and can propagate through the entire specimen as the global strain increases to 0.38, due to greater energy supplied by higher shear deformation in shear localization regions.

(3) The reaction product, determined by X-ray diffraction, is the intermetallic compound Ti_5Si_3 with a lattice parameter of $a = 7.35$ Å and $c = 5.48$ Å.

(4) Small triangular regions adjacent to the copper driver tube remain unreacted. This is the result of rapid cooling and arrest of reaction due to high thermal conductivity of copper. This region enables the calculation of the maximum reaction rate, $\sim 20\ s^{-1}$ at 1685 K, the melting point of Si.

(5) Since the reaction starts at localized shear strains ($\gamma = 10$), below the value leading to melting ($\gamma \sim 20$–40), it is proposed that there are temperature fluctuations, internal vortex formation, and interparticle friction that can initiate the reaction by a mechanism similar to Dremin and Breusov's [44] roller model. A solid state reaction mechanism [50] can also play an important role in the initiation of the reaction but in the experiments reported herein, it is impossible to separate the inputs from both mechanisms.

(6) The heat evolution due to intense shear localization propagates the exothermic reactions by forming liquid Si that surrounds fractured Ti particles. Spherical reaction particle products of Ti_5Si_3

form at the surface of Ti particles, and are expelled into the molten Si after they solidify.

Acknowledgements—This research was supported by the U.S. Army Research Office (Contracts DAAH04-94-G-0314 and DAAH04-95-1-0152) and by the Office of Naval Research (Contract N00014-94-1-1040). The authors gratefully acknowledge the support of E. Chen (ARO), J. Goldwasser (ONR), and R. Miller (ONR). Explosive experiments were carried out at the Institute of Hydrodynamics, Novosibirsk, Russia, by M.P. Bondar and Ya. L. Lukyanov, and at the Powder Metallurgy Research Institute, Minsk, Belarus, by S. Usherenko.

REFERENCES

1. Batsanov, S. S., *Effect of Explosions on Materials*. Springer, New York, 1994.
2. Graham, R. A., *Solids under High-Pressure Shock Compression*. Springer, New York, 1993.
3. Horie, Y., Sawaoka, A. B., *Shock Compression Chemistry of Materials*. KTK Scientific Publ., Japan, 1993.
4. DeCarli, P. S. and Jamieson, J. C., *Science*, 1961, **133**, 1821.
5. Thadhani, N. N., *Prog. Mater. Sci.*, 1993, **37**, 117.
6. Batsanov, S. S., *Mater. Sci. Engng*, 1996, **210A**, 57.
7. Krueger, B. R., Vreeland, T., Jr., in *Shock Waves and High Strain Rate Phenomena in Materials*, ed. M. A. Meyers, L. E. Murr and K. P. Staudhammer. Marcel Dekker, 1991, p. 242.
8. Krueger, B. R. and Vreeland, T. Jr., *J. appl. Phys.*, 1991, **69**(2), 710.
9. Krueger, B. R., Mutz, A. H. and Vreeland, T. Jr., *J. Appl. Phys.*, 1991, **70**(10), 5362.
10. Krueger, B. R., Mutz, A. M. and Vreeland, T. Jr., *Metall. Trans.*, 1992, **23A**, 55.
11. Yu, L. H., Meyers, M. A., in *Shock-Wave and High-Strain-Rate Phenomena in Materials*, ed. M. A. Meyers, L. E. Murr and K. P. Staudhammer. Marcel Dekker, New York, 1992, p. 303.
12. Meyers, M. A., Yu, L. H. and Vecchio, K. S., *Acta metall. mater.*, 1994, **42**(3), 715.
13. Vecchio, K. S., Yu, L. H. and Meyers, M. A., *Acta metall. mater.*, 1994, **42**(3), 701.
14. Batsanov, S. S., Marquis, F. D. S. and Meyers, M. A., in *Metall. and Mater. Applications of Shock-Wave and High-Strain-Rate Phenomena*, ed. L. E. Murr, K. P. Staudhammer and M. A. Meyers. Elsevier, Netherlands, 1995, p. 715.
15. Meyers, M. A., Batsanov, S. S., Gavrilkin, S. M., Chen, H. C., LaSalvia, J. C. and Marquis, F. D. S., *Mater. Sci. Engng A*, 1995, **201**, 150.
16. Vreeland, T. Jr., Montilla, K. and Mutz, A. H., *J. appl. Phys.*, 1997, **82**, 2840.
17. Bridgman, P. W., *J. Chem. Phys.*, 1947, **15**, 311.
18. Bridgman, P. W., *Phys. Rev.*, 1935, **48**, 825.
19. Bridgman, P. W., *Proc. Am. Acad. Arts Sci.*, 1937, **71**, 9.
20. Bridgman P. W., *The Physics of High Pressure*. Bell, London, 1949.
21. Vereshchagin, L. F., Zubova, E. V. and Burdina, K. P., *Dokl. Akad. Nauk. SSSR.*, 1966, **168**, 314.
22. Vereshchagin, L. F., Zubova, E. V. and Shapochkin, V. A., *Prib. Tekh. Eksp.*, 1960, **5**, 89.
23. Teller, E., *J. Chem. Phys.*, 1962, **36**, 901.
24. Enikolopyan, N. S., Mkhitaryan, A. A., Karagezyan, A. S. and Khzardzhyan, A. A., *Dokl. Akad. Nauk SSSR.*, 1987, **292**(4), 887.
25. Enikolopyan, N. S., *Pure appl. Chem.*, 1985, **57**(11), 1707.
26. Enikolopyan, N. S., *Russ. J. Phys. Chem.*, 1989, **63**(9), 1261.
27. Yu, L. H., Shock Synthesis and Synthesis-Assisted Consolidation of Aluminides and Silicides, Ph.D. Dissertation, New Mexico Institute of Mining and Technology, Socorro, NM, 1992.
28. Yu, L. H., Nellis, W. J., Meyers, M. A. and Vecchio, K. S., in *Shock Compression of Condensed Matter — 1993*, ed. S. C. Schmidt, J. W. Shaner, G. A. Samara and M. Ross. Am. Inst. Phys., 1994, p. 1291.
29. Potter, D. K. and Ahrens, T. J., *Geophys. Res. Lett.*, 1994, **21**, 721.
30. Nesterenko, V. F., Meyers, M. A., Chen, H. C. and LaSalvia, J. C., *Appl. Phys. Lett.*, 1994, **65**(24), 3069.
31. Nesterenko, V. F., Meyers, M. A., Chen, H. C. and LaSalvia, J. C., *Metall. Mater. Trans. A.*, 1995, **26**, 2511.
32. Nesterenko, V. F., Meyers, M. A., Chen, H. C. and LaSalvia, J. C., in *High-Pressure Science and Technology — 1995*, eds. S. C. Schmidt and W. C. Tao. Am. Inst. Phys., New York, 1996, p. 713.
33. Chen, H. C., Meyers, M. A. and Nesterenko, V. F., in *Metall. and Mater. Applications of Shock-Wave and High-Strain-Rate Phenomena*, ed. L. E. Murr, K. P. Staudhammer and M. A. Meyers, Elsevier, Netherland, 1995, p. 723.
34. Chase, M. W. Jr. , Davies, C. A., Downey, J. R., Jr., Frurip, D. J., McDonald, R. A. and Syverud, A. N., *J. Phys. Chem. Ref. Data*, 1985, **14** (Supplement No. 1, American Chemical Society and American Institute of Physics for the National Bureau of Standards, 1986).
35. Nesterenko, V. F., Lazaridi, A. N. and Pershin, S. A., *Fiz. Goreniya Vzryva*, 1989, **25**, 154.
36. Nesterenko, V. F., Bondar, M. P. and Ershov, I. V., in *High-Pressure Science and Technology — 1993*, ed. S. C. Schmidt, J. W. Shaner, G. A. Samara and M. Ross. Am. Inst. Phys., New York, 1994, p. 1172.
37. Love, A. E. H., *A Treatise on the Mathematical Theory of Elasticity*, 4th ed., Dover Publ., New York, 1944, pp. 33–34.
38. Nesterenko, V. F., Meyers, M. A. and Chen, H. C., *Acta mater.*, 1996, **44**(5), 2017.
39. LaSalvia, J. C., Kim, D. K., Lipsett, R. A. and Meyers, M. A., *Metall. Mater. Trans. A*, 1995, **26A**, 3001.
40. Johnson, G., Cook, W., *Proc. 7th Int. Symp. on Ballistics*, Hague, Netherlands, 1983, p. 955.
41. Bhaduri, S. B., Radhakrishnan, R. and Qian, Z. B., *Scripta metall. mater.*, 1992, **29**, 1089.
42. Bhaduri, S. B., *Scripta metall. mater.*, 1992, **27**, 1277.
43. Knacke, O., Kubashewski, O., Hesselmann, K., *Thermochemical Properties of Inorganic Substances*. Springer-Verlag, New York, 1991.
44. Dremin, A. N. and Breusov, O. N., *Russ. Chem. Rev.*, 1968, **37**(5), 392.
45. Merzhanov, A. G., *Fiz. Goreniya Vzryva*, 1973, **9**(1), 4.
46. Kosolapova, T. Ya., *Handbook of High Temperature Compounds: Properties, Production, Applications*. Hemisphere Publ., 1990.
47. Azatyan, T. S., Mal'tsev, V. M., Merzhanov, A. G. and Seleznev, V. A., *Comb. Explos. Shock Waves*, 1979, **15**, 35.
48. Dunmead, S. D., Munir, Z. A. and Holt, J. B., *J. Am. Ceram. Soc.*, 1992, **75**, 180.
49. Wang, L. L. and Munir, Z. A., *Metall. Mater. Trans.*, 1995, **26B**, 595.
50. Thadhani, N. N., Graham, R. A., Royal, T., Dunbar, E., Anderson, M. U. and Holman, G. T., *J. appl. Phys.*, 1997, **82**, 1113.